Submitted to the
International Europhysics Conference on High Energy Physics
Aachen, Germany, July 17 - 23, 2003

Abstract: 585 **Session: HQCD, HP**

The Q^2 dependence of dijet production at HERA

ZEUS Collaboration

13. June 2003

Abstract

The dependence of dijet production on the photon virtuality, Q^2, has been studied by measuring dijet cross sections in the range $0.1 < Q^2 < 2000$ GeV^2 with the ZEUS detector at HERA using an integrated luminosity of 38.6 pb^{-1}. Jets were identified in the hadronic centre-of-mass frame using the longitudinally invariant k_T cluster algorithm. The inclusive dijet cross sections were measured for jets with transverse energy $E_T^{\rm jet}$ above 7.5 GeV and 6.5 GeV and pseudorapidities in the hadronic centre-of-mass frame in the range $-3 < \eta^{\rm jet} < 0$. The results are presented as functions of Q^2, $E_T^{\rm jet1}$ and η^F, where $E_T^{\rm jet1}$ corresponds to the jet with the highest transverse energy and η^F is the pseudorapidity of the most forward jet. The ratio of dijet cross sections for $x_\gamma^{\rm obs}$ above 0.75 to those for $x_\gamma^{\rm obs}$ below 0.75, where $x_\gamma^{\rm obs}$ is the fraction of the photon momentum participating in the production of the dijet system, as a function of Q^2 and in different regions of $\overline{E}_T^2$ - the square of the average transverse energy of the two highest-transverse energy jets- has also been measured. NLO QCD calculations are compared to the measurements. The Q^2 dependence of the ratio of dijet cross sections, for which the theoretical uncertainties largely cancel, suggests a contribution from resolved photon processes may still be required for moderate Q^2.

1 Introduction

It has been established that the real photon ($Q^2 = 0$, where Q^2 is the virtuality of the photon) has a partonic structure [1–4], while at high Q^2, it is commonly considered to be a point-like particle and used as a probe of the partonic structure of hadronic targets [5–8]. Even though considerable progress from the theoretical [9–12] and experimental [13–16] sides has recently been made in investigating the structure of virtual photons, the parton distribution functions (PDFs) of the virtual photon are even less known than those of the real photon.

The structure of the virtual photon has been investigated by measurements of the photon structure function, $F_2^{\gamma^*}$, in $\gamma^*\gamma$ interactions at LEP [13,14]. At HERA, the virtual photon structure has been studied utilising jet production in $\gamma^* p$ interactions [15,16].

In this paper, the structure of the virtual photon is studied by means of dijet differential cross sections with respect to Q^2, $E_T^{\rm jet1}$ and η^F, where $E_T^{\rm jet1}$ is the jet with the highest transverse energy and η^F is the pseudorapidity of the most forward jet. The data sample used in this analysis corresponds to an eight-fold increase in luminosity with respect to the previous ZEUS study [16]. Next-to-leading-order (NLO) QCD calculations [17,18] have been compared for the first time to measurements that span a large range of photon virtualities.

Two processes contribute to the jet production cross section at leading order (LO) QCD [19, 20]: direct, in which the photon couples as a point-like particle to quarks; and resolved, in which the photon interacts via its partonic structure. Both processes lead to two jets in the final state. The $x_\gamma^{\rm obs}$ variable, which measures the fraction of the photon momentum participating in the production of the dijet system, is used to separate the two processes since resolved (direct) processes dominate at low (high) $x_\gamma^{\rm obs}$ values [21]. The variable $x_\gamma^{\rm obs}$ is defined as

$$x_\gamma^{\rm obs} = \frac{\sum_{\rm jets} E_T^{\rm jet} {\rm e}^{-\eta^{\rm jet}}}{2E_{\gamma^*}} \ ,$$

where the sum runs over the two jets with highest transverse energy and E_{γ^*} is the photon energy.

In studies of the virtual-photon structure using jet cross sections, two scales play a role: Q and the jet transverse energy, $E_T^{\rm jet}$. QCD predicts that, for high Q^2 ($Q^2 \gg E_T^{\rm jet}$), the resolved component will be suppressed and the photon will behave as a point-like particle. For $Q^2 \ll E_T^{\rm jet}$ the photon should have a partonic structure, even for relatively large values of Q^2. The ratio of cross sections for different ranges of $x_\gamma^{\rm obs}$ enhances the contribution of the resolved component, since the direct contribution is expected to be independent of Q^2. The measurements have been performed as a function of Q^2 in different regions of

$\overline{E}_T^2$, where $\overline{E}_T^2$ is the square of the average transverse energy of the two highest-transverse-energy jets.

2 Data selection and jet search

The dijet data sample was collected with the ZEUS detector during the 1996 and 1997 data-taking periods, in which HERA collided 820 GeV protons with 27.5 GeV positrons, and corresponds to an integrated luminosity of 38.6 ± 0.6 pb^{-1}. The ZEUS detector is described in detail elsewhere [22]. The most important components used in the current analysis were the uranium-scintillator (CAL) [23], the central tracking detector (CTD) [24] and the beam pipe calorimeter (BPC) [6]. The sample consists of sub-samples in two different Q^2 ranges:

- events at low Q^2 (LQS) were selected by requiring that the scattered positron was measured in the BPC. In this data set, the photon virtualities are in the range $0.1 < Q^2 < 0.55$ GeV^2.
- deep inelastic scattering (DIS) events were selected by requiring that the outgoing positron was measured in the CAL and the virtuality of the photon was required to be in the range $1.5 < Q^2 < 2000$ GeV^2.

For both subsamples, hadronic kinematic variables and jets were reconstructed using a combination of track and CAL information, known as energy-flow objects (EFOs), that optimises the reconstructed kinematic variables [25].

The EFOs were boosted to the hadronic centre-of-mass frame. The boost was calculated using the measured momentum of the scattered positron. The electron method [26] was used throughout this analysis to reconstruct the momentum of the scattered positron except when the angle of the hadronic system was less than 90° and the scattered positron track could be well reconstructed by the CTD. In this case, the Double Angle [26] method was used.

The measured cross sections refer to the phase-space region defined by $0.2 < y < 0.55$, where y is the inelasticity variable. The lower cut removes beam-gas interactions and the upper cut is imposed due to the restricted acceptance of the BPC detector. Additional cuts, similar to those described in an earlier publication [16], have been applied offline to select a clean sample of LQS and DIS events.

The k_T cluster algorithm [27] was applied to the boosted EFOs in the longitudinally invariant inclusive mode [28] to reconstruct jets in the hadronic final state. At least two jets are required in each event within the pseudorapidity range $-3 < \eta^{\rm jet} < 0$ and ordered

according to decreasing $E_T^{\rm jet}$. They were further required to satisfy $E_T^{\rm jet1} > 7.5$ GeV and $E_T^{\rm jet2} > 6.5$ GeV. After all cuts, the LQS (DIS) sample contained 2481 (45100) dijet events.

3 Data corrections and systematics

The data were corrected for detector acceptance and resolution using the HERWIG 5.9 [29] and PYTHIA 6.1 [30] Monte Carlo (MC) models. Fragmentation into hadrons is performed using the cluster model [31] in the case of HERWIG and the LUND [32] string model as implemented in JETSET [33,34] in the case of PYTHIA. Leading-order resolved (LO-RES) and direct (LO-DIR) processes were generated separately. The GRV LO [1] and MRSA [35] parametrization sets were used for the photon and proton PDFs, respectively.

The Monte Carlo events were processed through the full ZEUS detector simulation, based on the GEANT 3.13 [36] program, using the same cuts as applied to the data. The normalisations of the LO-RES and LO-DIR processes were extracted from the data using a two-parameter fit to the uncorrected $x_\gamma^{\rm obs}$ distributions. This procedure was applied separately for each Q^2 range.

The cross sections at hadron level were obtained by applying a bin-by-bin correction to the measured dijet distributions. The correction factors take into account the efficiency of the trigger, the selection criteria and the purity and efficiency of the jet reconstruction.

A detailed study of the sources contributing to the systematic uncertainties of the measurement was performed. The uncorrelated uncertainties were added in quadrature to the statistical error and are shown in the plots. The main source of correlated systematic uncertainties was the uncertainty on the absolute scale of the jets. Its effect on the dijet cross sections was approximately 9% at very low Q^2 and 6% at high Q^2. This uncertainty is shown in the plots as a band on the data. In addition, there is an overall normalisation uncertainty of 1.6% from the luminosity determination, which is not shown in the plots.

4 NLO QCD calculations

The NLO QCD calculations used in this analysis are based on the programs DISASTER++ [17] and DISENT [18] which compute jet production cross sections at NLO in the DIS regime. In these programs, the photon is treated as a highly virtual point-like probe and the programs do not include any contribution from resolved processes. DISENT and DISASTER++ make use of the subtraction method [37] for dealing with collinear and infra-red divergencies and are performed in the massless $\overline{\rm MS}$ renormalisation and factorisation schemes. A comparison between DISASTER++ and DISENT shows that they

agree within ±3%. In Section 5 only the calculations using DISASTER++ are compared to the data because this program allows a wider parameter selection than DISENT.

For the calculations presented here, the number of flavours was set to 5, the renormalisation and factorisation scales were set to $\mu^2 = \mu_R^2 = \mu_F^2 = Q^2 + (E_T^{\rm jet})^2$ or Q^2 and $\alpha_s(\mu_R)$ was calculated at two loops using $\Lambda^{(5)}_{\overline{\rm MS}} = 226$ MeV, which corresponds to $\alpha_S(M_Z) = 0.118$. The CTEQ5M1 [38] sets were used for the proton PDFs. The scale Q^2 is not a sensible choice for $Q^2 < (E_T^{\rm jet})^2$ but the calculations with this scale have been shown in the plots over the whole Q^2 range for completeness.

The predictions compared with the data were corrected using a bin-by-bin procedure for hadronisation effects according to $d\sigma = d\sigma^{\rm NLO} \cdot C_{\rm had}^{-1}$, where $d\sigma^{\rm NLO}$ is the cross section for partons in the final state of the NLO calculation. The hadronisation correction factor was defined as the ratio of the dijet cross sections before and after the hadronisation process, $C_{\rm had} = d\sigma_{\rm MC}^{\rm partons}/d\sigma_{\rm MC}^{\rm hadrons}$. The value of $C_{\rm had}$ was taken as the mean of the ratio obtained using the ARIADNE and LEPTO predictions for the calculations and was found to lie between 1.1 (large Q^2) and 1.2 (small Q^2).

5 Results

Figures 1 and 2 presents the differential dijet cross section, $d\sigma/dQ^2$, for $E_T^{\rm jet1} > 7.5$ GeV, $E_T^{\rm jet2} > 6.5$ GeV, $-3 < \eta^{\rm jet} < 0$ and $0.2 < y < 0.55$ in the range $0.1 < Q^2 < 2000$ GeV^2 for the direct-enhanced region ($x_\gamma^{\rm obs} > 0.75$) and the resolved-enhanced region ($x_\gamma^{\rm obs} < 0.75$), together with the total dijet cross section. The measurements cover a wide range of photon virtualities with precision. The measured cross sections fall by more than four orders of magnitude over this Q^2 range. The cross section for $x_\gamma^{\rm obs} < 0.75$ falls more rapidly than that for $x_\gamma^{\rm obs} > 0.75$. Even though the total cross section is dominated by interactions with $x_\gamma^{\rm obs} > 0.75$ for $Q^2 \gtrsim 10$ GeV^2, there is still a contribution of approximately 24% from low-$x_\gamma^{\rm obs}$ events even for Q^2 as high as ~ 500 GeV^2. The NLO QCD calculations using DISASTER++ with $\mu_R^2 = Q^2 + (E_T^{\rm jet})^2$ and $\mu_R^2 = Q^2$ are compared to the measured $d\sigma/dQ^2$ in Figs. 1 and 2, respectively. The prediction[1] with $\mu_R^2 = Q^2 + (E_T^{\rm jet})^2$ describes the shape of the measured total dijet cross section but underestimates its magnitude by approximately 30%, whereas the prediction with $\mu_R^2 = Q^2$ is within 10% of the measurement except for the lowest bin of the calculation where it overestimates the data by around 30%. The measured cross section for $x_\gamma^{\rm obs} > 0.75$ is reasonably well described by the calculation shown in fig. 1a for all Q^2; the prediction in fig. 2 describes the measured cross section for $Q^2 > 10$ GeV^2 but for lower Q^2 values it overestimates the measurement

[1] The lowest Q^2 bin is outside the range of applicability of the DISASTER++ program.

even though consistent within the large renormalisation scale uncertainty. The prediction with $\mu_R^2 = Q^2 + (E_T^{\rm jet})^2$ underestimates the measured cross section for $x_\gamma^{\rm obs} < 0.75$ even at low Q^2, whereas the calculation with $\mu_R^2 = Q^2$ is in better agreement with the data.

The calculations shown give an estimate of the uncertainty due to the choice of the renormalisation scale. In addition, the uncertainty coming from the missing higher orders, which was estimated by varying the value of μ_R in each choice, for $\mu_R^2 = Q^2$ can be as high as 100% at low Q^2. Taking into account all uncertainties, only the cross section for $x_\gamma^{\rm obs} > 0.75$ is well described by the calculation. A possible explanation of the disagreement at low $x_\gamma^{\rm obs}$ values is that the effects from the structure of the photon are expected in this region, where the contribution predicted by DISASTER++ comes only from large-angle particle-emission diagrams included in the NLO corrections to the dijet cross section.

Figure 3 shows the dijet cross section, $d^2\sigma/dQ^2dE_T^{\rm jet1}$, as a function of $E_T^{\rm jet1}$ in different Q^2 ranges. The measurements extend up to transverse energies of approximately 40 GeV. The $E_T^{\rm jet1}$ distribution falls less steeply as Q^2 increases. Figure 3 also shows the calculations of DISASTER++. In the region $1.5 < Q^2 < 4.5$ GeV^2 for large jet transverse energies, where the dominant scale might be expected to be $E_T^{\rm jet}$, the calculation with Q as the scale is seen to significantly exceed the measured cross section whereas that with $\mu_R^2 = Q^2 + (E_T^{\rm jet})^2$ is in better agreement. As Q^2 increases, particularly in the high Q^2 region, $120 < Q^2 < 2000$ GeV^2 the calculations with both $\mu_R^2 = Q^2$ and $\mu_R^2 = Q^2 + (E_T^{\rm jet})^2$ are in better agreement with each other and with the data.

The differential cross-section $d^2\sigma/dQ^2d\eta^F$ as a function of η^F is shown in Fig. 4 for different ranges of Q^2. The cross section as a function of $\eta^{\rm jet}$ is more sensitive to the resolved photon component in the forward direction[2]. In all Q^2 regions, the measured cross section increases with η_F in the region from -2.5 to -1.5. For $\eta^F > -1.5$, the cross section decreases as η^F increases for $Q^2 \gtrsim 10$ GeV^2, whereas at low Q^2 the cross section increases. At low Q^2, the NLO QCD prediction with $\mu_R^2 = Q^2$ again lies above the data for all η_F although that with $\mu_R^2 = Q^2 + (E_T^{\rm jet})^2$ underestimates the measured cross section in the forward direction, the data lying between the two. As Q^2 increases, again both calculations are seen to be in better agreement with each other and the data, although both still lie below the data for forward η_F.

The Q^2 dependence of the direct- and resolved-enhanced components of the dijet cross section has been studied in more detail using the ratio

$$R = \frac{{\rm d}\sigma}{{\rm d}Q^2}(x_\gamma^{\rm obs} < 0.75)/\frac{{\rm d}\sigma}{{\rm d}Q^2}(x_\gamma^{\rm obs} > 0.75).$$

[2] Since η here is defined in the hadronic center-of-mass frame, the forward region in the laboratory frame corresponds to $\eta > -1$.

The experimental and theoretical uncertainties largely cancel in this ratio, so that the presence of a resolved contribution can be investigated. Figure 5 shows the ratio R as a function of Q^2 in three different regions of $\overline{E}_T^2$. The Q^2 dependence of the data is stronger at low $\overline{E}_T^2$, where the photon is expected to have structure, than for higher $\overline{E}_T^2$, showing that the resolved contribution is suppressed at low Q^2 as $\overline{E}_T^2$ increases.

The NLO DIS calculations describe the Q^2 dependence of the measured ratio except for low $\overline{E}_T^2$ and Q^2. This suggests that calculations may need to include a contribution from resolved photon processes even for scales as high as $Q^2 \sim 10$ GeV^2 and $49 < \overline{E}_T^2 < 85$ GeV^2.

6 Summary and conclusions

Dijet differential cross sections have been measured in the kinematic range defined by $0.1 < Q^2 < 2000$ GeV^2, $0.2 < y < 0.55$, $-3 < \eta^{\rm jet} < 0$ and $E_T^{\rm jet\,1,jet2} > 7.5$ and 6.5 GeV, as a function of Q^2, $E_T^{\rm jet1}$ and η^F in the hadronic-centre-of-mass frame. The precise measurements spanning a large range of photon virtualities, can significantly constrain the parton densities in the virtual photon.

Present next-to-leading-order QCD calculations have large uncertainties at low Q^2, where the presence of a resolved photon contribution is expected. Improved higher-order or resummed calculations are needed. The uncertainties in the ratio of the dijet cross sections as a function of Q^2 for $x_\gamma^{\rm obs} \lesssim 0.75$ largely cancel, and suggest calculations may need to include resolved photon processes for scales as high as $Q^2 \sim 10$ GeV^2 and $49 < \overline{E}_T^2 < 85$ GeV^2.

Acknowledgements

The design, construction and installation of the ZEUS detector have been made possible by the ingenuity and dedicated efforts of many people from inside DESY and from the home institutes who are not listed as authors. Their contributions are acknowledged with great appreciation. The experiment was made possible by the inventiveness and the diligent efforts of the HERA machine group. The strong support and encouragement of the DESY directorate have been invaluable.

References

[1] M. Glück, E. Reya and A. Vogt, Phys. Rev. **D 46**, 1973 (1992).

[2] H. Abramowicz, K. Charchula and A. Levy, Phys. Lett. **B 269**, 458 (1991).

[3] L.E. Gordon and J.K. Storrow, Nucl. Phys. **B 489**, 405 (1997).

[4] P. Aurenche, J.P. Guillet and M. Fontannaz, Z. Phys. **C 64**, 621 (1994).

[5] ZEUS Coll., M. Derrick et al., Z. Phys. **C 72**, 399 (1996).

[6] ZEUS Coll., J. Breitweg et al., Phys. Lett. **B 407**, 432 (1997).

[7] H1 Coll., S. Aid et al., Nucl. Phys. **B 470**, 3 (1996).

[8] H1 Coll., C. Adloff et al., Nucl. Phys. **B 497**, 3 (1997).

[9] J. Chyla and M. Tasevsky, Phys. Rev. **D 62**, 114025 (2000).

[10] K. Sasaki and T. Uematsu, Nucl. Phys. Proc. Suppl. **B 89**, 162 (2000).

[11] M. Krawczyk and A. Zembrzuski, Nucl. Phys. Proc. Suppl. **B 82**, 167 (2000).

[12] B. Pötter, Nucl. Phys. Proc. Suppl. **B 82**, 145 (2000).

[13] OPAL Coll., G. Abbiendi et al., Eur. Phys. J. **C 24**, 17 (2002).

[14] L3 Coll., M. Acciarri et al., Phys. Lett. **B 438**, 363 (1998).

[15] H1 Coll., C. Adloff et al., Eur. Phys. J. **C 13**, 397 (2000).

[16] ZEUS Coll., J. Breitweg et al., Phys. Lett. **B 479**, 37 (2000).

[17] D. Graudenz, Preprint hep-ph/9710244, 1997.

[18] S. Catani and M.H. Seymour, Nucl. Phys. **B 485**, 291 (1997).

[19] C.H. Llewellyn Smith, Phys. Lett. **B 79**, 83 (1978);
I. Kang and C.H. Llewellyn Smith, Nucl. Phys. **B 166**, 413 (1980);
J.F. Owens, Phys. Rev. **D 21**, 54 (1980);
M. Fontannaz, A. Mantrach and D. Schiff, Z. Phys. **C 6**, 241 (1980).

[20] W.J. Stirling and Z. Kunszt, *Proc. HERA Workshop*, R. Peccei (ed.), Vol. 1, p. 331. DESY (1987);
M. Drees and F. Halzen, Phys. Rev. Lett. **61**, 275 (1988);
M. Drees and R.M. Godbole, Phys. Rev. Lett. **61**, 682 (1988);
M. Drees and R.M. Godbole, Phys. Rev. Lett. **39**, 169 (1989);
H. Baer, J. Ohnemus and J.F. Owens, Z. Phys. **C 42**, 657 (1989);
H. Baer, J. Ohnemus and J.F. Owens, Phys. Rev. **D 40**, 2844 (1989).

[21] ZEUS Coll., M. Derrick et al., Phys. Lett. **B 322**, 287 (1994).

[22] ZEUS Coll., U. Holm (ed.), *The ZEUS Detector*. Status Report (unpublished), DESY (1993), available on `http://www-zeus.desy.de/bluebook/bluebook.html`.

[23] M. Derrick et al., Nucl. Inst. Meth. **A 309**, 77 (1991);
A. Andresen et al., Nucl. Inst. Meth. **A 309**, 101 (1991);
A. Caldwell et al., Nucl. Inst. Meth. **A 321**, 356 (1992);
A. Bernstein et al., Nucl. Inst. Meth. **A 336**, 23 (1993).

[24] N. Harnew et al., Nucl. Inst. Meth. **A 279**, 290 (1989);
B. Foster et al., Nucl. Phys. Proc. Suppl. **B 32**, 181 (1993);
B. Foster et al., Nucl. Inst. Meth. **A 338**, 254 (1994).

[25] G.M. Briskin, *Diffractive Dissociation in ep Deep Inelastic Scattering*. Ph.D. Thesis, Tel Aviv University, 1998. (Unpublished).

[26] S. Bentvelsen, J. Engelen and P. Kooijman, *Proc. Workshop on Physics at HERA*, W. Buchmüller and G. Ingelman (eds.), Vol. 1, p. 23. Hamburg, Germany, DESY (1992).

[27] ZEUS Coll., J. Breitweg et al., Eur. Phys. J. **C 1**, 109 (1998).

[28] S.D. Ellis and D.E. Soper, Phys. Rev. **D 48**, 3160 (1993).

[29] G. Marchesini et al., Comp. Phys. Comm. **67**, 465 (1992).

[30] T. Sjöstrand, Comp. Phys. Comm. **82**, 74 (1994).

[31] B.R. Webber, Nucl. Phys. **B 238**, 192 (1984).

[32] B. Andersson et al., Phys. Rep. **97**, 31 (1983).

[33] T. Sjöstrand, Comp. Phys. Comm. **39**, 347 (1986).

[34] T. Sjöstrand and M. Bengtsson, Comp. Phys. Comm. **43**, 367 (1987).

[35] A.D. Martin, R.G. Roberts and W.J. Stirling, Phys. Rev. **D 50**, 6734 (1994).

[36] R. Brun et al., GEANT3, Technical Report CERN-DD/EE/84-1, CERN, 1987.

[37] R.K. Ellis, D.A. Ross and A.E. Terrano, Nucl. Phys. **B 178**, 421 (1981).

[38] H.L. Lai et al., Phys. Rev. **D 55**, 1280 (1997).

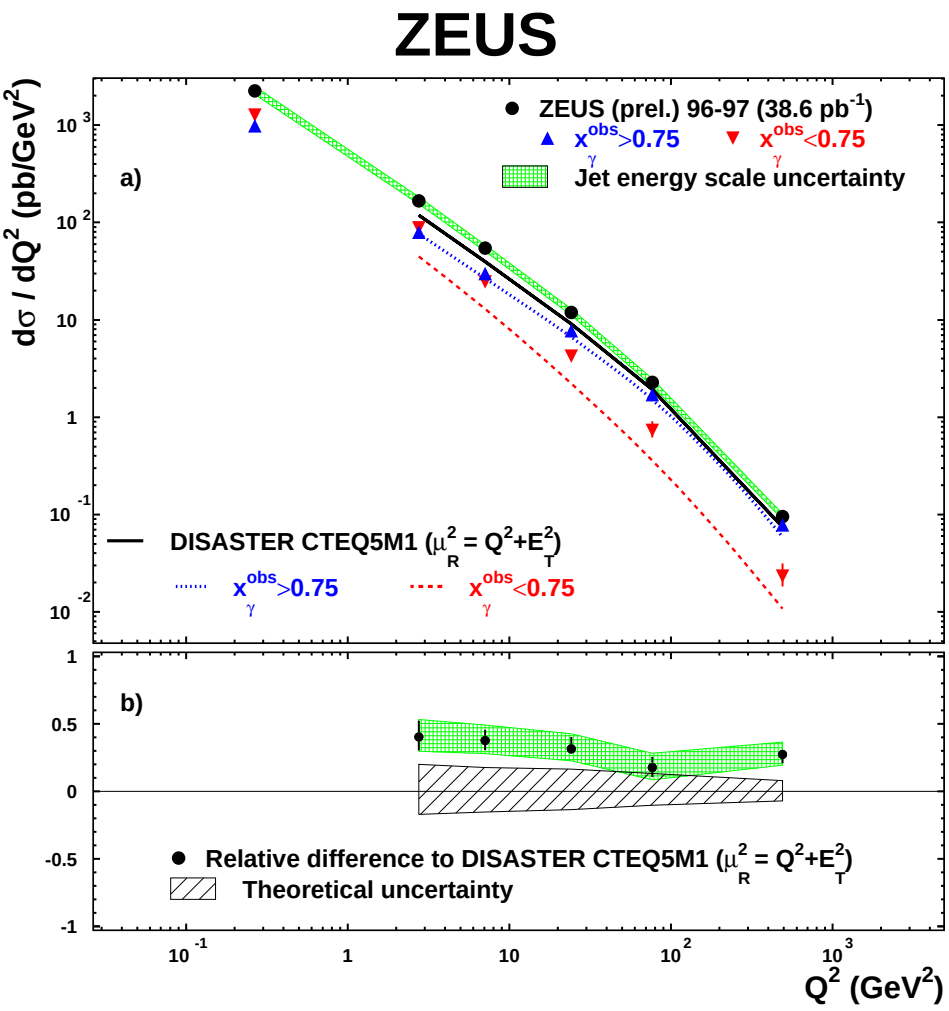

Figure 1: *a) Measured dijet cross-sections $d\sigma/dQ^2$ for $x_\gamma^{\rm obs} > 0.75$ (upwards triangles) $d\sigma/dQ^2$ for $x_\gamma^{\rm obs} < 0.75$ (downwards triangles) and $d\sigma/dQ^2$ for the whole $x_\gamma^{\rm obs}$ region (black dots). The inner vertical bars represent the statistical uncertainties of the data, and the outer bars show the statistical and systematic uncertainties added in quadrature, except for that associated with the uncertainty in the absolute energy scale of the jets (shaded band). The NLO QCD calculations of DISASTER++ with $\mu_R^2 = Q^2 + (E_T^{\rm jet})^2$ are shown for each of the cross-sections. b) Relative difference of the measured dijet cross-section $d\sigma/dQ^2$ to the DISASTER++ calculation with $\mu_R^2 = Q^2 + (E_T^{\rm jet})^2$. The hatched band shows the theoretical uncertainty of the calculation.*

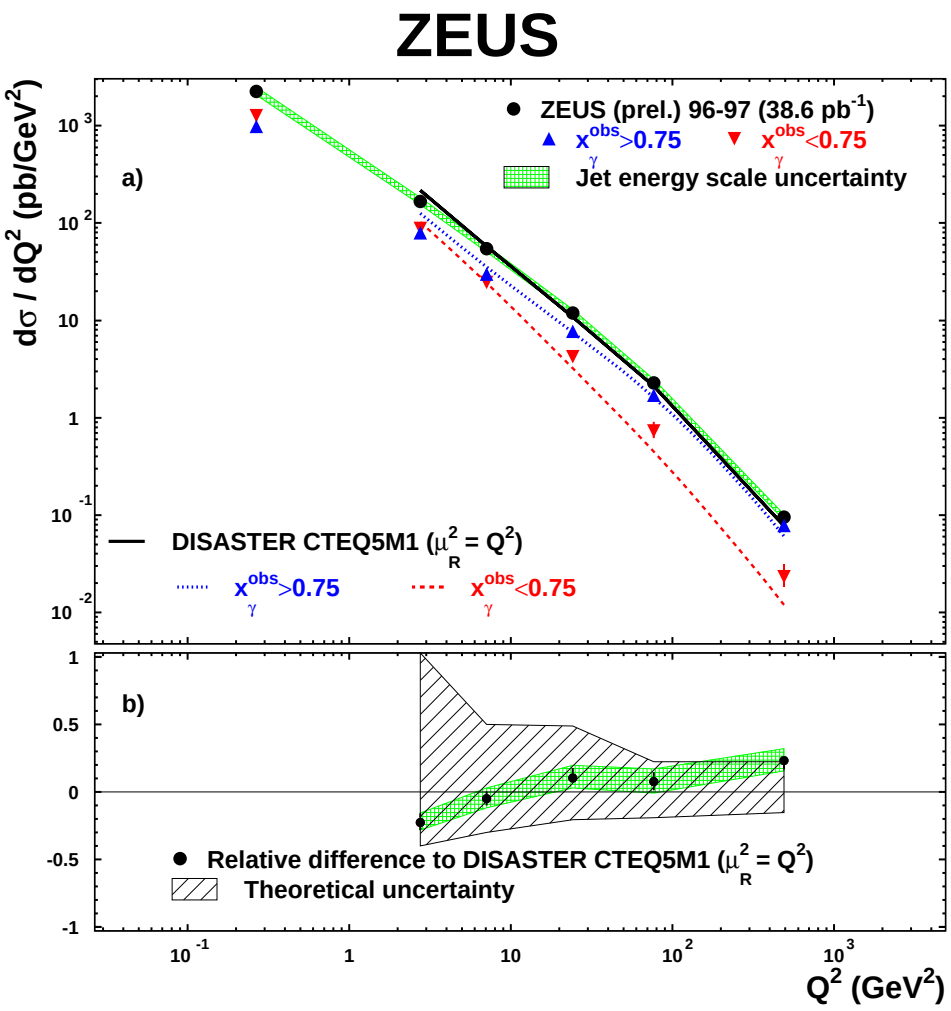

Figure 2: *a) Measured dijet cross-sections $d\sigma/dQ^2$ for $x_\gamma^{\rm obs} > 0.75$ (upwards triangles) $d\sigma/dQ^2$ for $x_\gamma^{\rm obs} < 0.75$ (downwards triangles) and $d\sigma/dQ^2$ for the whole $x_\gamma^{\rm obs}$ region (black dots). The inner vertical bars represent the statistical uncertainties of the data, and the outer bars show the statistical and systematic uncertainties added in quadrature, except for that associated with the uncertainty in the absolute energy scale of the jets (shaded band). The NLO QCD calculations of DISASTER++ with $\mu_R^2 = Q^2$ are shown for each of the cross-sections. b) Relative difference of the measured dijet cross-section $d\sigma/dQ^2$ to the DISASTER++ calculation with $\mu_R^2 = Q^2$. The hatched band shows the theoretical uncertainty of the calculation.*

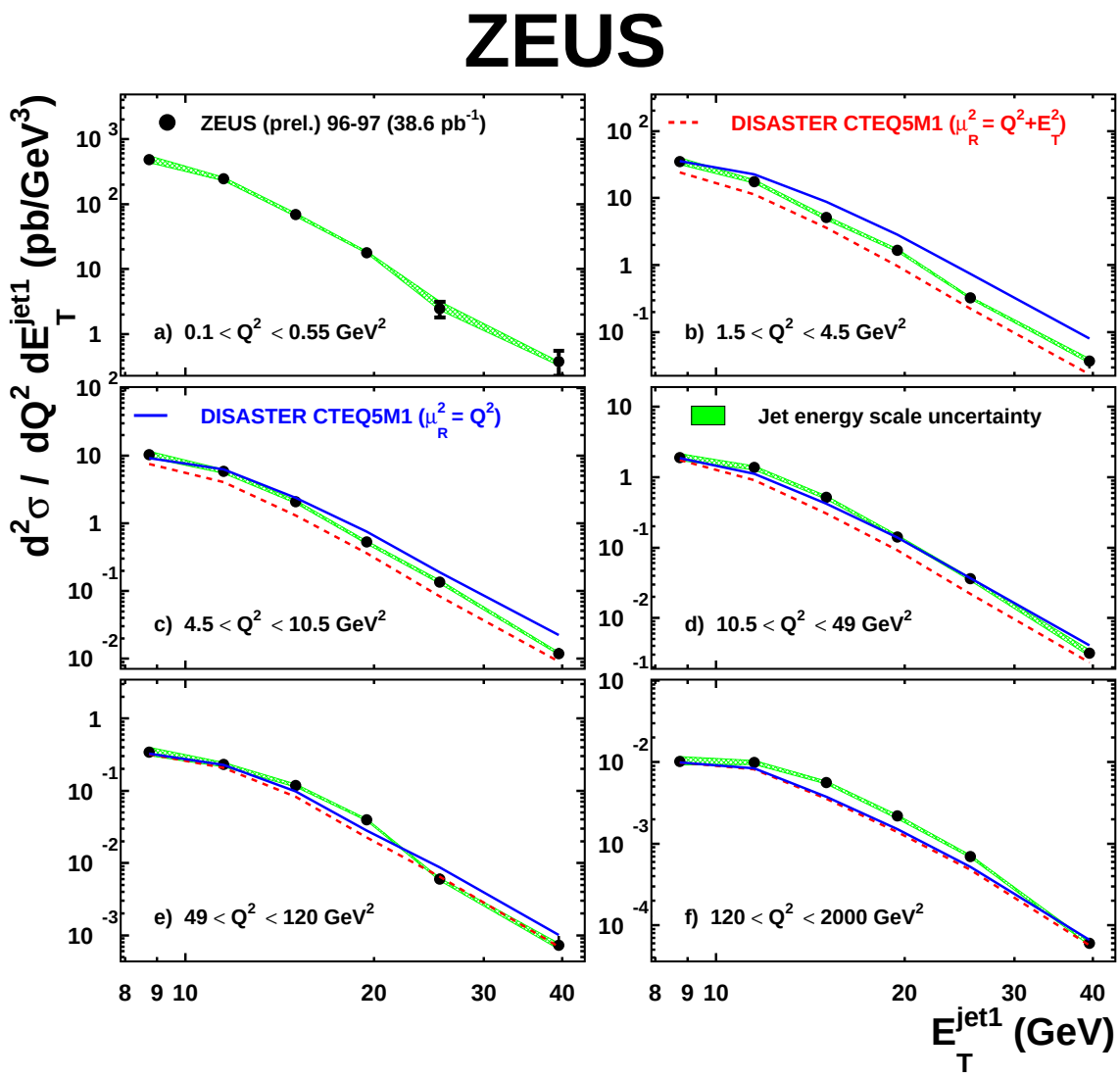

Figure 3: *Measured dijet cross-section $d^2\sigma/dQ^2dE_T^{\rm jet1}$ (black dots). The NLO QCD calculations of DISASTER++ with $\mu_R^2 = Q^2 + (E_T^{\rm jet})^2$ (dashed line) and $\mu_R^2 = Q^2$ (solid line) are also shown. Other details as in the caption to Fig. 1.*

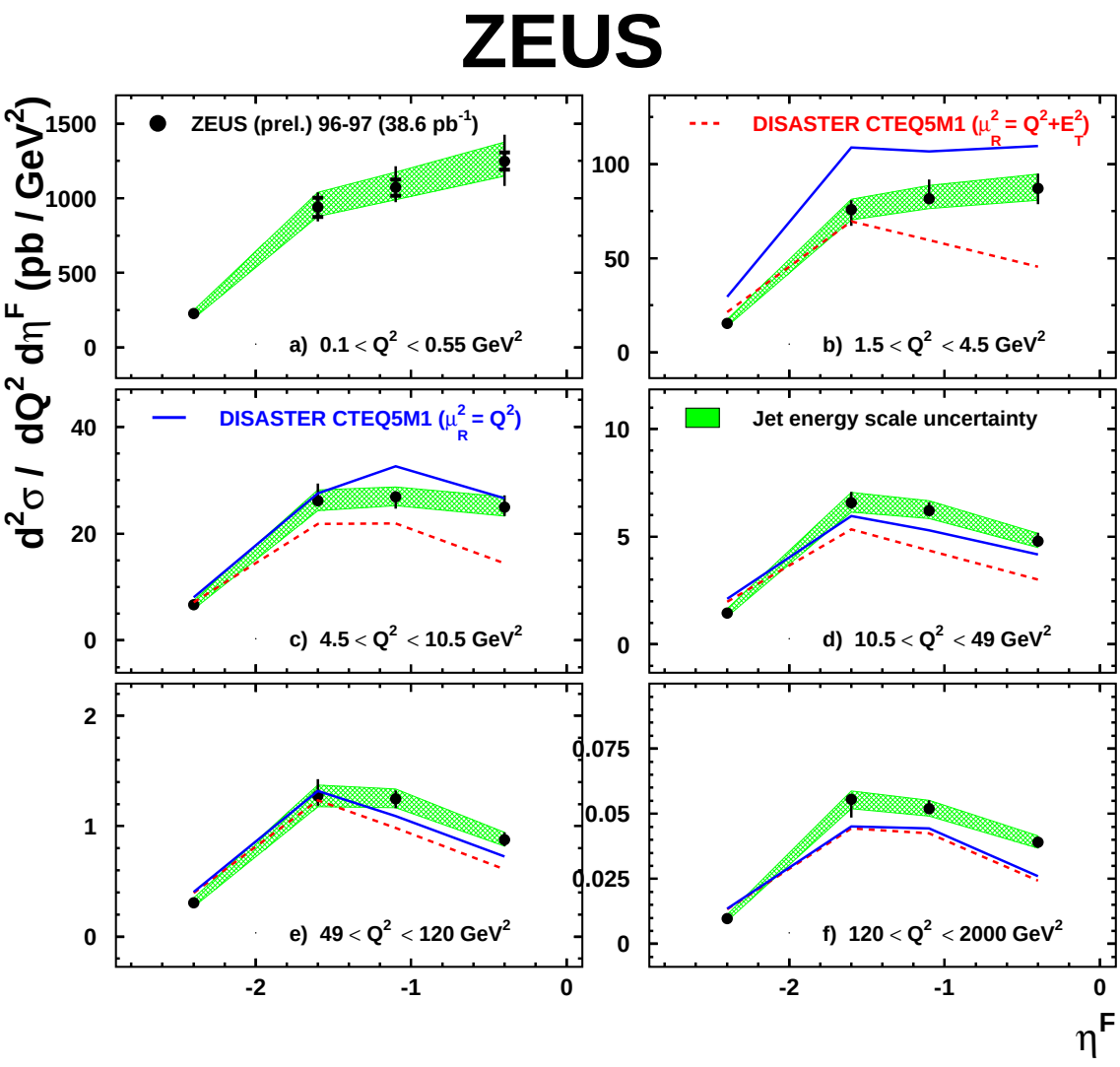

Figure 4: *Measured dijet cross-section $d\sigma/dQ^2 d\eta^F$ (black dots). The NLO QCD calculations of DISASTER++ with $\mu_R^2 = Q^2 + (E_T^{\rm jet})^2$ (dashed line) and $\mu_R^2 = Q^2$ (solid line) are also shown. Other details as in the caption to Fig. 1.*

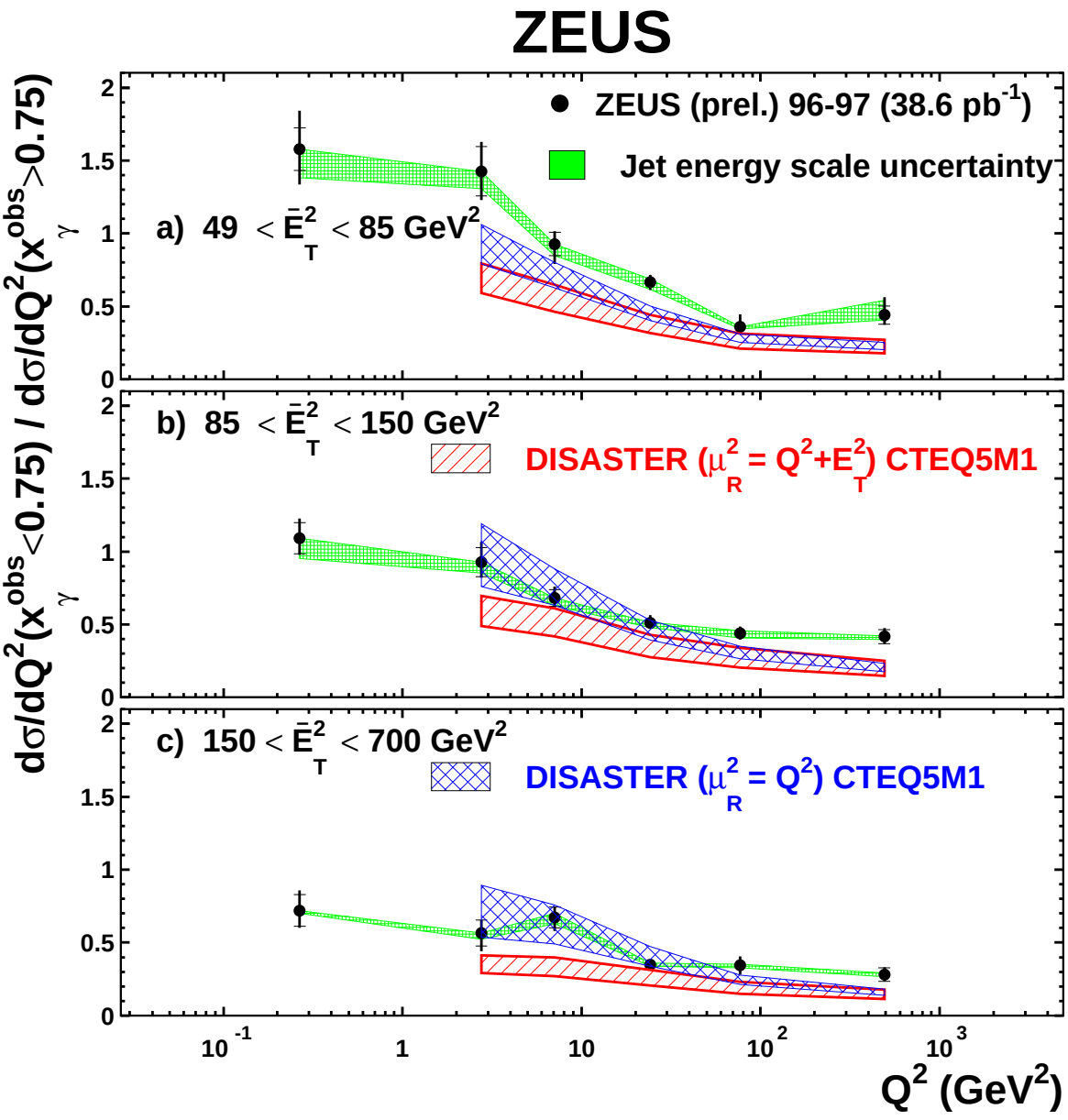

Figure 5: *Measured ratio* $R = \frac{d\sigma}{dQ^2}(x_\gamma^{\rm obs} < 0.75)/\frac{d\sigma}{dQ^2}(x_\gamma^{\rm obs} > 0.75)$ *as a function of* Q^2 *in different regions of* $\overline{E}_T^2$ *(black dots). The NLO QCD calculations of DISASTER++ with* $\mu_R^2 = Q^2 + (E_T^{\rm jet})^2$ *and* $\mu_R^2 = Q^2$ *are also shown. The hatched bands represent the theoretical uncertainties. Other details as in the caption to Fig. 1.*